An Energy-Efficient Multi-Channel Charge Trackable Inductor-Based Stimulation System

Eojin Kim[1] and Chul Kim[a]
Department of Bio and Brain Engineering, Korea Advanced Institute of Science and Technology
E-mail : [1]eojin@kaist.ac.kr

Abstract **- The concept of "electroceuticals" has recently emerged, aiming to maximize therapeutic effects by delivering targeted electrical stimulation while minimizing side effects. To realize electroceuticals, it is essential to develop implantable stimulators that meet specific requirements, such as overcoming battery size limitations, ensuring safety, and providing effective electrical stimulation. Therefore, these stimulators must operate with high energy efficiency and have the capability to monitor the amount of charge delivered to the body. However, existing electrical stimulators fail to meet these requirements. Therefore, this study developed a Charge Trackable Inductor-Based Stimulator (CTIBS) that achieves up to 80% of peak stimulator efficiency, with a charge error between anodic and cathodic stimulation being less than 1.6%. Additionally, the number of stimulation channels has been expanded to 16, allowing for flexible control over the stimulation area and density. The integrated circuit (IC) chip was designed using a 180 nm RF process, occupying an area of 5 mm².**

Keywords**—Electric Stimulator, Energy-Efficient, Charge-Trackable, Multi-Channel**

I. INTRODUCTION

Traditional treatments, including surgical procedures and pharmacological therapies, often lead to post-operative complications and adverse effects on other organs [1]. In order to overcome these side effects, the concept of ‘ electroceuticals' has recently been in the spotlight.

Electroceuticals accurately target specific nerve cells or neural circuits and apply electrical stimulation to restore lost body function or correct physical dysfunction. Since electrical stimulation is applied only to the desired area, the effect of treatment is maximized, but side effects are minimized. In addition, since the form of electrical stimulation can be customized for the patient, personalized treatment is possible [2].

There are many medical fields that try to use electric drugs for the treatment. A pacemaker, which is used to correct cardiac abnormalities, is a representative example of electro drug. [3]. Besides, many studies are conducted to expand the usage of electro drugs, such as spinal cord stimulation (SCS), deep brain stimulation (DBS), Parkinson's disease, epilepsy, vagus nerve stimulation, muscle and nerve rehabilitation [4-8].

In order to realize the electroceuticals, a stimulator must be inserted into the body. In the case of the implantable stimulator currently used, a large battery is relied on to supply power to the device in the body. However, it is difficult to insert a large volume of the battery in areas where internal space is insufficient, such as the brain. Therefore, a cable line connecting the body and the battery outside for power supply and data processing is inevitable [9]. The external cable line causes discomfort to users, and challenges the non-human or primate experiment [10]. If the stimulator can be operated in a low power environment, the volume of the battery will be effectively reduced and the method can be used in various areas.

When stimulating tissue, it is important to control the amount of charge delivered to the cells. The amount of charge transferred determines whether the tissue is stimulated or not [11]. Also, the process of recovering the charge as much as the transferred amount of charge is required. Through this process, the charge stored in the electrodes and cells can be discharged. This prevents from electrode corrosion and tissue damage by the charge accumulates [12]. Thus, tracking stimulation charge is essential for the safe and effective operation of the electronic medicine system.

This work aims to develop Charge Trackable Inductor-Based Stimulator (CTIBS), which is energy-efficient and can track the stimulation charge. The energy-efficient stimulation was implemented by the free-wheeling characteristic of an external inductor. The charge tracking function was realized by an on-chip capacitor. In addition, to control the stimulation area and density [13], H-bridge structure is used achieving 16-channel expansion. The peak stimulator efficiency was 80%, and the charge balancing error was within 1.6%. The IC chip was designed in RF 180nm process, taking up the area of 5mm^2

a. Corresponding author; kimchul@kaist.ac.kr

Manuscript Received Aug. 23, 2024, Revised Nov. 11, 2024, Accepted Dec. 9, 2024

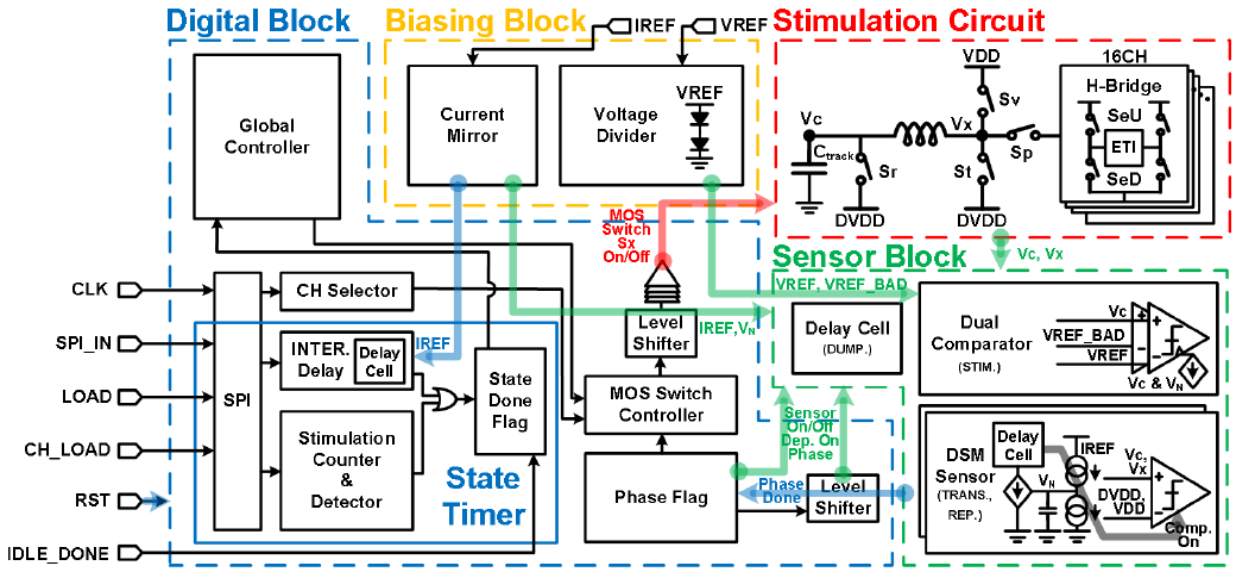

Fig. 1. The entire block diagram of the proposed system.

II. DESIGN METHODOLOGY

A. *Entire System Structure*

The entire block diagram of the proposed system structure is shown in Fig. 1. The system is largely divided into four blocks according to the system hierarchy and function. The four blocks include a digital block, a biasing block, a sensor block, and a stimulation circuit.

These four blocks proceed with 4 states and 4 stimulation phases through interaction. The four states consist of an idle state (IDLE), an intermediate delay state (INTER), and cathodic/anodic stimulation state (CAT/AN_STIM). During cathodic/anodic stimulation states, the stimulation current is sent from/to the tissue. Each stimulation state consists of four phases, which grants energy-efficient stimulation and charge tracking ability to the proposed stimulator. The four phases consist of stimulation phase (STIM), transfer phase (TRAN), replenishing phase (REP), and dump phase (DUMP). The whole cycle of 4 phases are repeated until the stimulation charge meets the target amount.

B. *Charge Trackable Inductor-Based Stimulator (CTIBS)*

The diagram of the CTIBS is shown in Fig. 2. CTIBS consists of 16 H-bridge stimulation channels that are directly connected to the stimulation capacitor, inductor, MOS switches, and electrode-tissue model. The MOS switches are controlled by commands transmitted from the digital circuit and the sensor block according to the four states of the system and the four phases of the stimulation state. It has a high-efficiency structure that measures the amount of stimulation charge using a stimulation capacitor and uses an inductor to return the excess energy remaining in the stimulation circuit to the supply.

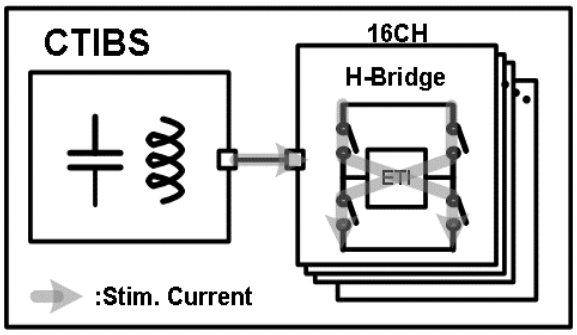

Fig. 2. The block diagram of the Charge Trackable Inductor-Based Stimulator (CTIBS).

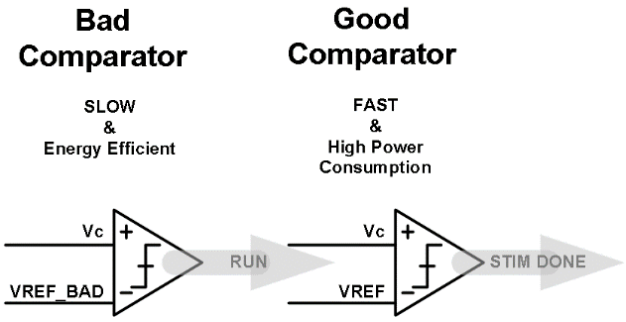

Fig. 3. The block diagram of a dual comparator.

C. *Double Comparator Phase Control*

To determine the phases during cathodic/anodic stimulation state, the sensor block needs to interact with CTIBS. In the case of the STIM phase, the phase duration was adjusted using a double comparator. The diagram of the double comparator is shown in Fig. 3.

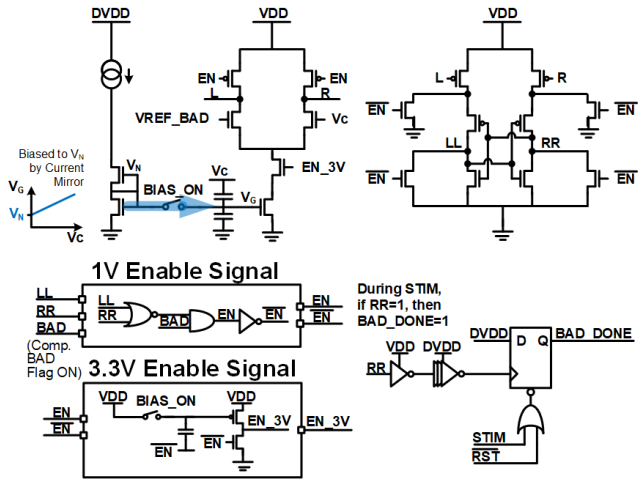

Fig. 4. The circuit instrument of the self-clocked dynamic comparator.

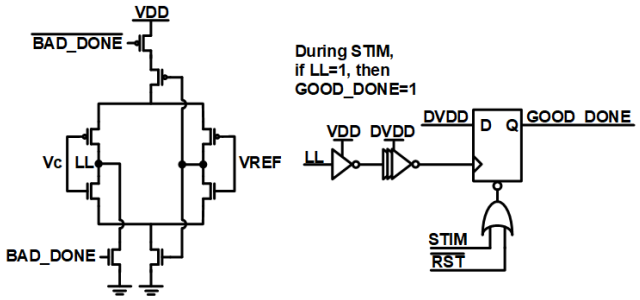

Fig. 5. The circuit instrument of the self-clocked dynamic comparator.

During STIM phase, the stimulation current is sent from/to the target tissue. As the stimulating phase is repeated, the charges accumulate in the double layer capacitor of the electrode. This changes the amplitude of the stimulation current, and thus the duration taken to bring/send the same amount of charge changes significantly. However, the end point of the stimulation phase must be accurately determined, as it is a factor that directly determines the effectiveness of the charge tracking function of the system. Therefore, a comparator that can make an accurate judgment regardless of duration is needed.

For the comparator to make an accurate judgment, it should have a high time resolution. However, the frequent judgment causes great amount of energy consumption. Therefore, to solve this problem, two comparators were used. The one operates in slow speed but consumes low energy. This was realized by a self-clocked dynamic comparator [14], whose clock speed depends on the voltage level of sensing point. The other operates in fast speed, but consumes lots of energy, which was realized by a continuous comparator.

When the STIM phase begins, the self-clocked dynamic comparator compares the sensing point with VREF_BAD. The circuit instrument is shown in Fig. 4. VREF_BAD is a voltage created by five diodes connected in series between VREF and DVDD, equivalent to VREF minus one-fifth of

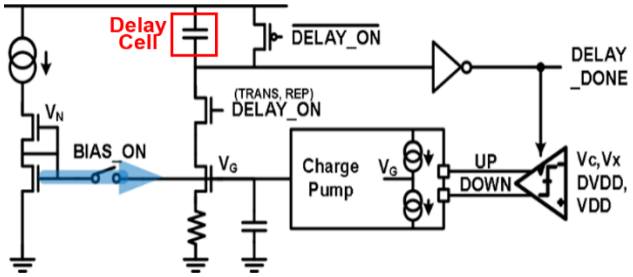

Fig 6. The block diagram of ΔΣ Delay Cell Modulation (DSM) sensor.

the difference. The comparator operates slowly at first, but as the sensing voltage approaches VREF_BAD, the comparation speed increases. Once the sensing point reaches VREF_BAD, the self-clocked dynamic comparator stops and triggers the continuous comparator.

The circuit instrument of the continuous comparator is shown in Fig.5. The continuous comparator, operating in the hundreds of MHz range, compares the sensing point with VREF. When the sensing reaches VREF, the comparator stops and generates signal to end the STIM phase. Using these two comparators in series, it was able to make a comparator block that works accurately and energy-efficiently.

D. ΔΣ Delay Cell Modulation (DSM) Sensor Phase Control

In the case of the TRANS and REP phase, ΔΣ delay cell modulation (DSM) sensor determines the duration. The diagram of DSM sensor is shown in Fig.6.

The duration of TRANS and REP do not change significantly even after several repeated cycles. Thus, the Δ Σ delay cell was used which saves the duration time and adjusts it by a charge pump. This operates in energy-efficient way, because the comparator only needs to judge once during the phase.

A bias voltage V_N is generated in the current mirror. This voltage is transmitted to V_G by a MOS switch operated by the BIAS_ON signal. The BIAS_ON signal is only received when the system is first operated.

The capacitor and the dependent current source are connected and work as an adjustable delay cell. During DELAY_ON, either when it is TRANS or REP phase signal is on, the dependent current source charges the capacitor. When the capacitor voltage exceeds the threshold of the inverter, the DELAY_ON signal is turned off, discharging the capacitor, and moving on to the next phase.

The charge pump adjusts the current level of the dependent current source. According to the information transmitted from the comparator, it increases or decreases V_G. For the fast determination of phase duration, digital logic was implemented, which integrates the error information in the flip-flop cell.

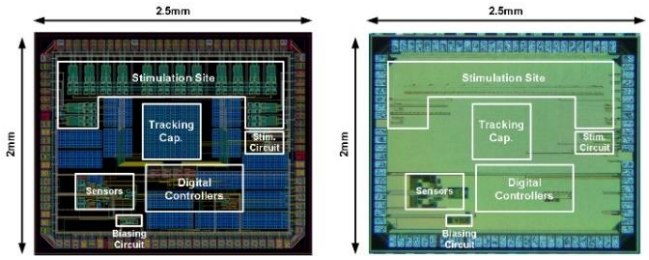

(a) (b)

Fig 7. (a) The layout of the designed integrated circuit and (b) microscopic picture.

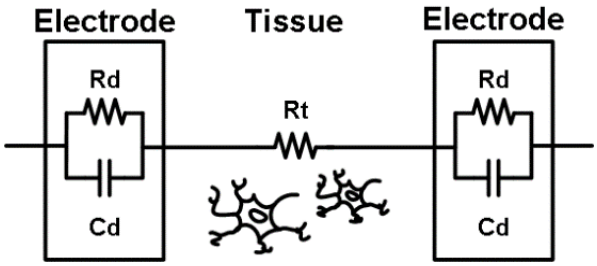

Fig. 8. Electrode-tissue interference model (ETI).

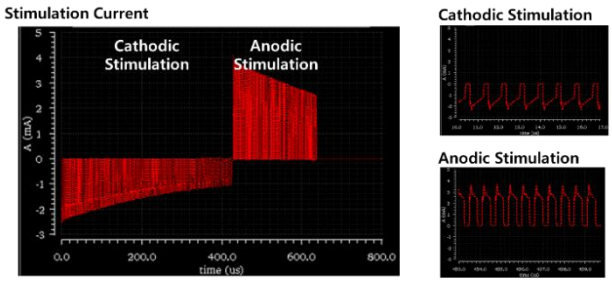

Fig. 9. The waveform of stimulation current.

A degenerative resistor is placed at the source terminal of the dependent current source, in order to increase the linearity of the current change according to V_G.

III. RESULTS AND DISCUSSIONS

A. *Chip Layout*

The integrated circuit was designed in TSMC 180nm RF CMOS process, with the size is 2.5mm x 2mm, an area of 5 ㎟. In the Fig.7, the layout picture of the circuit is on the left and the microscopic picture is on the right.

B. *The Simulation Validation of Circuit Operation*

Fig. 7 shows the current flowing through the electrode-tissue model. The model values were set as R_t=1kΩ, R_d=10MΩ, and C_d=500nF (Fig. 8). The target stimulation charge was set to 300nC.

In Fig.9, the current flows in the negative direction during cathodic stimulation, and the current flows in the positive direction during anodic stimulation. When cathodic stimulation

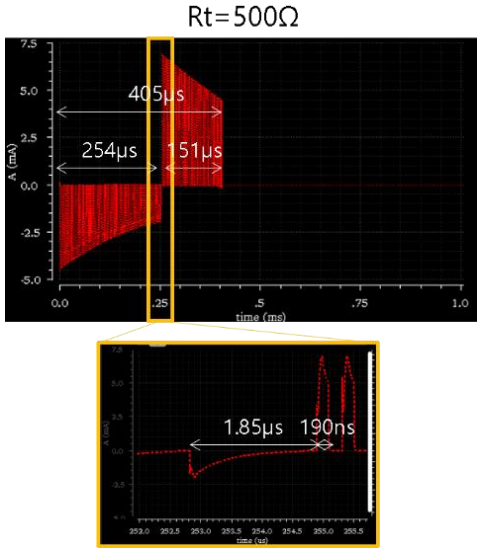

Fig. 10. The waveform of stimulation current when R_t = 500Ω.

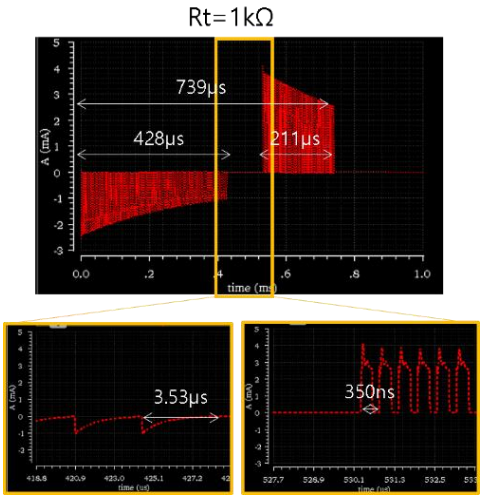

Fig.11. The waveform of stimulation current when R_t = 1kΩ.

occurs, the electrode double layer capacitor (C_d) is gradually filled with charge. Therefore, the waveform shows wide and shallow shape, the relatively small current flows with longer duration. However, when anodic stimulation occurs, the relatively large current flows rapidly due to the electric charges charged in Cd. The current waveform has a narrow and deep shape. This phenomenon occurs because the charge accumulated in Cd had realized as a certain amount of voltage.

Fig. 10 − Fig. 12 show the stimulation current waveform as the tissue resistance (R_t) changes. When the tissue resistance is small, stimulation current flows relatively large and rapidly, forming a narrow and deep waveform. Therefore, as the tissue resistance increases, the time it takes to complete the stimulation becomes longer and the intensity of the stimulation current decreases.

Fig. 13 shows the operation of dual comparator. The double comparator should determine the end point of STIM phase, when Vc meets target voltage 2V. As a result, it was

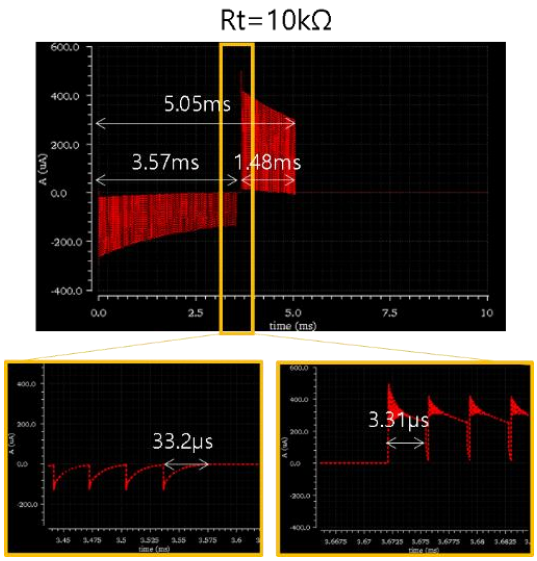

Fig. 12. The waveform of stimulation current when R_t = 10kΩ.

confirmed that the STIM phase flag was turned off as soon as Vc reached 2V. This means that the double comparator operated desirably.

The DSM sensor controls the duration of TRAN and REP phases. Fig. 14 shows the DSM sensor operation during TRAN phase as a sample. Initially, the delay created by the delay cell may deviate from the target time length. However, as phase repeats, a desirable delay time should be created.

To evaluate the adjusting ability of DSM sensor, an initial offset error was intentionally applied to the speed of discharging delay cell. This was realized by setting the value of the gate voltage (V_G) of the dependent current deviated from the preferred value. At the top of Fig. 14, V_G over time is shown. The value of V_G was initially set higher than the optimal level. But, as time goes by, it gradually went down and converged the desirable level as the phase was repeated. The bottom of Fig. 14 shows the Vc value over time. During TRAN phase, the DSM sensor should determine the end point of the phase, when Vc meets target voltage 1V. When V_G did not converge, the phase ended before Vc reaching 1V, which is not desirable. However, after the phase repeated and V_G converged, TRAN flag turned off when Vc reached 1V, which is desirable. This means that the DSM sensor integrated the error well to create the desired delay time.

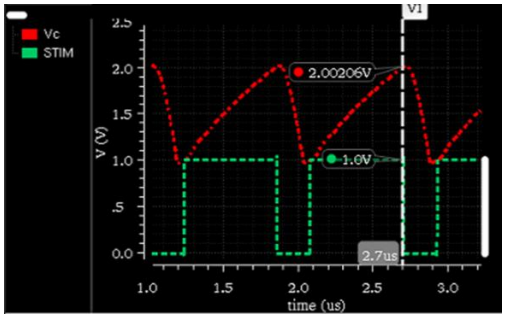

Fig. 13. The operation of dual comparator.

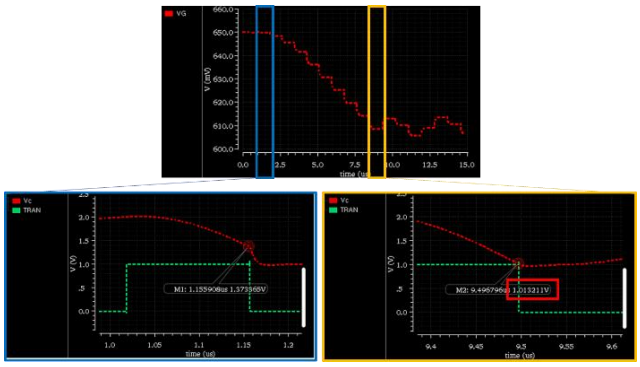

Fig. 14. The operation of DSM sensor.

TABLE I. The Accuracy of Charge Tracking: Delivered Stimulation Charge.

R_t	Target Charge	Delivered Charge	Error
500Ω	300nC	318.12nC	6.04%
1kΩ		316.66nC	5.55%
10kΩ		315.02nC	5.01%

C. *Charge Tracking and Charge Balance*

The experiment is conducted to find out how well the system tracks the delivered stimulation charge. Table I shows how much the actual amount of charge delivered deviated from the target value during cathodic stimulations. The value of R_t was set to 500Ω, 1kΩ, and 10kΩ. The target stimulation charge was 300 nC. As a result, it was confirmed that the amount of stimulation charge actually delivered to the tissue was about 5~6% more than the target value.

TABLE II. The Accuracy of Charge Tracking: Charge Balance.

R_t	Cathodic Stimulation	Anodic Stimulation	Residuals				Error	
			B/F Passive		A/F Passive		B/F Passive	A/F Passive
			Charge	Voltage	Charge	Voltage		
500Ω	318.12nC	319.06nC	944pC	3.76mV	4.10fC	16.4nV	0.29%	0%
1kΩ	316.66nC	314.80nC	1.86nC	7.26mV	86.3aC	345pV	0.59%	0%
10kΩ	315.02nC	310.07nC	4.95nC	19.8mV	3.63fC	14.51nV	1.57%	0%

$$\eta_{Stimulation} = \frac{P_{Tissue}}{P_{StimulationCircuit}} = \frac{E_{Tissue}}{E_{StimulationCircuit}}$$

Equ. 1. The stimulation efficiency.

$$\eta_{Stimulator} = \frac{P_{Tissue}}{P_{System}} = \frac{E_{Tissue}}{E_{System}}$$

Equ. 2. The stimulator efficiency.

TABLE Ⅲ. The Stimulation Efficiency.

R_t		
500Ω	1kΩ	10kΩ
1.073μJ / 1.273μJ → 84.3%	1.101μJ / 1.280μJ → 86.0%	1.115μJ / 1.277μJ → 87.3%

TABLE Ⅳ. The Stimulator Efficiency.

R_t		
500Ω	1kΩ	10kΩ
1.073μJ / 1.343μJ → 80.1%	1.101μJ / 1.384μJ → 79.6%	1.115μJ / 2.028μJ → 55.0%

In order to prevent an electrode or tissue from being damaged, the charge balance between cathodic and anodic stimulation is important. Table II compares the actual charge amount delivered during cathodic stimulation with anodic stimulation. It also shows the charge error before and after the passive charge balancing which was conducted during IDLE. The experiment was conducted by setting R_t to 500Ω, 1 kΩ, and 10 kΩ. The target stimulation charge was 300nC. The external signal to end the IDLE occurred every 10ms.

As a result, an error up to 1.6% occurred just before IDLE started. This is an error amount to about 5nC, which was expressed as a residual voltage of about 20mV. However, when the passive charge balancing continued in IDLE, an error was close to 0%.

D. *Efficiency*

The stimulation efficiency refers to the efficiency of a stimulation circuit. The definition is equal to Equ. 1. The result of the experiment is shown in Table III, demonstrating stimulation efficiency was from 84.3% to 87.3 for R_t values of 500Ω, 1kΩ, and 10kΩ.

The stimulator efficiency refers to the efficiency of the entire system. The definition of stimulator efficiency is equal to Equ. 2. The result of the experiment is shown in Table IV, demonstrating stimulator efficiency was from 80.1 % to 55.0 % for R_t values of 500Ω, 1kΩ, and 10kΩ.

Fig. 15 shows the ratio of the energy consumed by the main blocks of the system and tissue. The experiment was conducted by setting R_t to 500Ω, 1kΩ, and 10KΩ. The target stimulation charge was 300 nC.

Under all conditions, the energy consumed by the tissue accounted for more than half of the total energy consumed

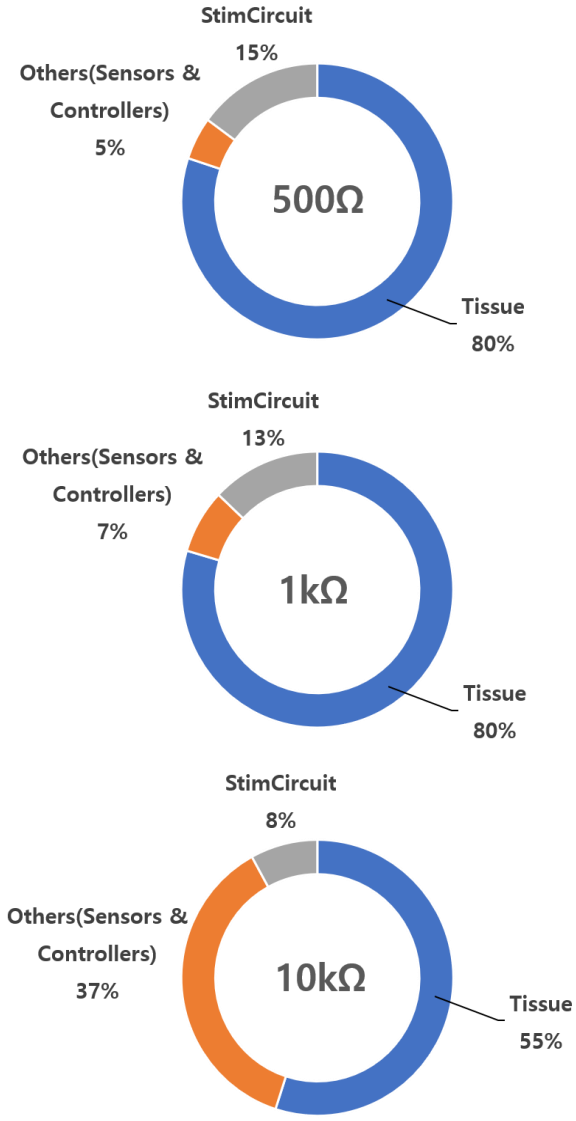

Fig 15. The energy usage ratio respect to tissue resistance.

by the system. When tissue resistance was 500Ω or 1 kΩ, it showed a remarkable stimulator efficiency of almost 80%. However, when the tissue resistance was 10kΩ, the stimulator efficiency dropped to 55%, and it was confirmed that most of the energy was consumed by the sensor block.

E. *Performance Comparison*

Table V compares the proposing work with the previous works. This work is designed in 0.18μm process. The system operates in 1V and 3.3V supply. The stimulation current was up to 8mA. The number of stimulation channel is expanded to 16, and the stimulator peak efficiency is increased to 80%. The target load range is between 500Ω and 10kΩ which is wide. The residual voltage after the biphasic stimulation was smaller than 20mV.

TABLE V. Performance Comparison.

Performance	This work	[15]	[16]
Process	0.18µm	0.18µm	0.18µm
Operating Voltage	3.3V, 1V	3.5V	0V - 12V
Channels	16	8	1
Stimulation Current	< 8mA	<18mA	0.2m – 3mA
Stimulator Peak Efficiency	80%	68%	37%
Target Load	500Ω - 10kΩ	0.5kΩ	2kΩ
Residual Voltage	< 20mV	-	118.9mV

IV. CONCLUSION

This study proposes a 16-channel stimulator system that is energy-efficient and capable of tracking stimulation charges. This system satisfies the key requirements for an electrical stimulator, including miniaturization, high energy efficiency, precise charge tracking, and support for multi-channel operation. The peak stimulator efficiency was 80%, and the charge balancing error was within 1.6%. The IC chip was designed in RF 180nm process, taking up the area of 5mm^2.

ACKNOWLEDGMENT

The chip fabrication was supported by the IC Design Education Center (IDEC), Korea.

REFERENCES

[1] Seicol, Benjamin J., et al. “Neuromodulation of metabolic functions: from pharmaceuticals to bioelectronics to biocircuits.” Journal of biological engineering 13.1 (2019): 1-12
[2] Mishra, Sundeep. “Electroceuticals in medicine–The brave new future.” Indian Heart Journal 69.5 (2017): 685-686.
[3] Medtronic, "The Adapta™" (n.d.)
[4] Medtronic, "PERCEPT™ PC " (n.d.)
[5] Sdrulla, Andrei D., Yun Guan, and Srinivasa N. Raja. "Spinal cord stimulation: clinical efficacy and potential mechanisms." Pain Practice 18.8 (2018): 1048-1067.
[6] Benabid, Alim Louis. "Deep brain stimulation for Parkinson’s disease." Current opinion in neurobiology 13.6 (2003): 696-706.
[7] Ben-Menachem, Elinor. "Vagus-nerve stimulation for the treatment of epilepsy." The Lancet Neurology 1.8 (2002): 477-482.
[8] Alonso-Alonso, Miguel, Felipe Fregni, and Alvaro Pascual-Leone. "Brain stimulation in poststroke rehabilitation." Cerebrovascular diseases 24.Suppl. 1 (2007): 157-166.
[9] Muller, Rikky, et al. “A minimally invasive 64-channel wireless µECoG implant.” IEEE Journal of Solid-State Circuits 50.1 (2014): 344-359.
[10] Chang, Yonghee, et al. “Seamless Capacitive Body Channel Wireless Power Transmission Toward Freely Moving Multiple Animals in an Animal Cage.” IEEE Transactions on Biomedical Circuits and Systems 16.4 (2022): 714-725.
[11] Noble, D., and R. B. Stein. “The threshold conditions for initiation of action potentials by excitable cells.” The Journal of Physiology 187.1 (1966): 129-162.
[12] Merrill, Daniel R., Marom Bikson, and John GR Jefferys. “Electrical stimulation of excitable tissue: design of efficacious and safe protocols.” Journal of Neuroscience Methods 141.2 (2005): 171-198.
[13] Cho, Jaeouk, et al “Energy-Efficient Integrated Circuit Solutions Toward Miniaturized Closed-Loop Neural Interface Systems.” Frontiers in Neuroscience 15 (2021): 667447.
[14] Kim, Hongkyun, Yechan Park, and Chul Kim. "A 13.56-MHz Wireless Power Transfer System with a Wide Operating Distance and Load Range for Biometric Smartcards." IEEE Transactions on Power Electronics 38.4 (2022): 5576-5585.
[15] Urso, Alessandro, et al. "An Ultra High Frequency 8 Channel Neurostimulator Circuit With 68% Peak Power Efficiency." IEEE transactions on biomedical circuits and systems 13.5 (2019): 882 892.
[16] Z. Luo et al., "A High Voltage Tolerant and Precise Charge Balanced Neuro Stimulator in Low Voltage CMOS Process," IEEE TBioCAS, (2016)

Eojin Kim received the B.S. degree in Biomechatronics from Sungkyunkwan University (SKKU), Suwon, Republic of Korea, in 2022 and M.S. degree in Bio and Brain Engineering from Korea Advanced Institution of Science and Technology (KAIST), in 2024. She is currently pursuing the Ph.D. degree in Bio and Brain Engineering from KAIST. Her research interests include integrated circuit (IC) chip design for energy-efficient circuit design, biomedical healthcare system, and neural stimulator.

Chul Kim (Senior Member, IEEE) is an associate professor in the Department of Bio and Brain Engineering and the Program of Brain and Cognitive Engineering at Korea Advanced Institute of Science and Technology (KAIST), Daejeon, South Korea. He received the Ph.D. degree in bioengineering, UC San Diego, La Jolla, CA, USA, in 2017 where he was a postdoctoral fellow from 2017 to 2019. From 2009 to 2012, he was with SK HYNIX, Icheon, South Korea, where he designed power management circuitry for dynamic random-access memory (DRAM). His current research interests include the design of energy-efficient integrated circuits and systems for fully wireless brain-machine interfaces and unobtrusive wearable sensors.